Mon. Not. R. Astron. Soc. **315**, 521–533 (2000)

Towards a model for the solar dynamo

David Moss[1]★ and John Brooke[1,2]
[1]*Mathematics Department, University of Manchester, Manchester M13 9PL*
[2]*Manchester Computing, University of Manchester, Manchester M13 9PL*

Accepted 2000 January 24. Received 2000 January 24; in original form 1999 May 26

ABSTRACT

We study a mean field model of the solar dynamo, in which the non-linearity is the action of the azimuthal component of the Lorentz force of the dynamo-generated magnetic field on the angular velocity. The underlying zero-order angular velocity is consistent with recent determinations of the solar rotation law, and the form of the alpha effect is chosen so as to give a plausible butterfly diagram. For small Prandtl numbers we find regular, intermittent and apparently chaotic behaviour, depending on the size of the alpha coefficient. For certain parameters, the intermittency displays some of the characteristics believed to be associated with the Maunder minimum. We thus believe that we are capturing some features of the solar dynamo.

Key words: magnetic fields – MHD – Sun: activity – Sun: magnetic fields.

1 INTRODUCTION

In spite of intensive study, one of the basic problems of astrophysical magnetohydrodynamics remains unsolved in detail: namely, we do not have a completely satisfactory model for the behaviour of the large-scale solar magnetic field. The consensus now is that a hydromagnetic dynamo operates, driven by the differential rotation and some effect of the cyclonic turbulence, and cyclic behaviour has been readily produced by dynamo models since the work of Parker (1955) and Steenbeck, Krause & Rädler (1966).

When looked at it in more detail, the solar surface magnetic field displays only a quasi-periodic behaviour, the '22-yr cycle', probably with a longer period modulation (e.g. the 'Gleissberg cycle').This longer modulation appears in both the length and the amplitude of the '22-yr cycle'. In addition there are intervals where the overall level of magnetic activity is considerably reduced, the 'grand minima'. Such a reduction in solar magnetic activity leads to a higher production rate of cosmogenic isotopes such as ^{10}Be and ^{14}C, owing to a reduction in the shielding effect of the solar wind. Examination of various fossil records indicates that such intervals of reduced activity have occurred repeatedly over the last 10 000 years (Struiver & Braziunas 1989). The only such episode to have occurred since telescopic observation of the Sun began is the Maunder minimum during the late 17th and early 18th centuries. This was marked by a great reduction in the number of sunspots. However, evidence from the ^{10}Be record indicates that the basic magnetic cycle continued through this period (Beer, Tobias & Weiss 1998). There is thus some uncertainty as to what a grand minimum episode involves, and this is of considerable theoretical importance, in that several papers have recently been published that claim to model grand minima by a variety of mechanisms that are physically and mathematically very distinct: modulation by deterministic chaos (e.g. Knobloch, Tobias & Weiss 1998), stochastic modulation (e.g. Schmitt, Schüssler & Ferriz-Mas 1996), or a novel form of intermittency variously termed 'icicle' or 'in–out' intermittency (e.g. Brooke et al. 1998; Ashwin, Covas & Tavakol 1999). We return to this point in Sections 2 and 9.

The sunspots, and so by inference the subsurface magnetic field, exhibit the well-known 'butterfly diagram' – i.e. the main region of sunspot occurrence moves from mid-latitudes to near the equator during each half-cycle. There is also a weaker polar branch, in which the field migration is poleward. The global magnetic field is normally of approximately odd symmetry with respect to the equator (odd parity or dipole-like), but there is also an even-parity component present (e.g. Verma 1993; Pulkkinen et al. 1999 and references therein), and a quadrupole-like component may have been dominant during the Maunder minimum (Ribes & Nesme-Ribes 1993; Sokoloff & Nesme-Ribes 1994).

The other observational input to the problem that has recently become available is the determination of the internal solar rotation law (e.g. Kosovichev et al. 1997; also Christensen-Dalsgaard & Schou 1988; Tomczyk, Schou & Thompson 1995). In contrast to the rotation laws assumed in a number of earlier dynamo models, there is only a weak radial dependence of the angular velocity through the bulk of the solar convection zone, combined with a narrow tachocline near the base, where the angular velocity makes a transition to that of the approximately uniformly rotating interior. Another calibration of the model is given by the requirement that the mean cycle period be approximately 22 yr. Many earlier models have tended to ignore this requirement, possessing periods that can be shorter by as much as an order of magnitude. A more detailed discussion of the location of and

★ E-mail: moss@ma.man.ac.uk

mechanisms involved in a solar dynamo model is given in Rüdiger & Brandenburg (1995), and will not be repeated here.

Previous studies have addressed various aspects of the problem. There are too many references to give a comprehensive list here, but recent relevant work includes Rüdiger & Brandenburg (1995), Charbonneau & MacGregor (1997), Tobias (1997, hereafter T97), Küker, Arlt & Rüdiger (1999, hereafter KAR) and Pipin (1999). The model of T97 was further discussed in Knobloch et al. (1998). Rüdiger & Brandenburg used alpha-quenching and buoyancy non-linearities, with anisotropic diffusivity and alpha tensors, in spherical geometry with a realistic solar rotation law. The model of T97 was more idealized, using Cartesian geometry, with a velocity shear depending only on the quasi-radial coordinate. The non-linearity was the effect of the Lorentz force on the velocity shear. Both of these models had comparatively thick overshoot regions, with radial extent comparable to that of the overlying convection zone (that of T97 could be interpreted as straddling the bottom of the convection zone). Charbonneau & MacGregor (1997) also used a quasi-solar rotation law, in spherical geometry, with a diffusivity in the relatively narrow overshoot region that was much smaller than that in the convection zone. Their models were linear. KAR and Pipin (1999) used a parametrization of the turbulent Reynolds stresses ('Λ-effect') to generate the underlying rotational shear. They included non-linearities caused both by Λ-quenching and by the Lorentz force acting on the rotational shear, in spherical geometry. In KAR, the basic rotation law was radially dependent, but Pipin (1999) included a more realistic form. Also, Roald & Thomas (1997) studied the effects of algebraic alpha- and omega-quenching in a quasi-one-dimensional model, and Tobias (1996) discussed the effects of a reduction of the magnetic diffusivity in the presence of strong magnetic fields near the bottom of the convection zone.

It remains the case that no published global model possesses simultaneously a realistic butterfly diagram and an approximately solar rotation law, together with multi-periodicity, the persistent presence of a small quadrupolar field component, and irregular intervals of reduced overall field strength when the quadrupolar field component becomes relatively more important, although all of these features can be found singly or in restricted combinations in the literature.

In this paper we examine a relatively unsophisticated model for the solar dynamo. We want to move away from the more idealized type of model, and with that in mind we use spherical geometry, and include a more realistic representation of the solar rotation law. [Moss (1999) has studied other consequences of such a rotation law.] In our model, the field is limited at finite amplitude solely by the effect of the azimuthal component of the dynamo-generated Lorentz force on the underlying differential rotation. As we consider the angular velocity to be known approximately, we choose a form of the alpha coefficient of mean field theory that ensures a plausible butterfly diagram. Our model is also calibrated by the requirement that the cycle period be of the correct order of magnitude.

2 QUESTIONS OF PARITY

A particular aspect of the solar dynamo problem that has recently excited considerable interest is the relation between fluctuations of energy and parity in dynamo models. This is motivated by the evidence that the distribution of sunspots during the Maunder minimum was highly asymmetric with respect to the equator (Ribes & Nesme-Ribes 1993). Unfortunately we have at present no means of assessing the symmetry of the solar field before 1600, thus it is impossible to tell if this coincidence of abnormally low energy and asymmetry is typical of solar grand minima. The same considerations apply a fortiori to the grand minima inferred to occur in one-third of solar-type stars (Balunias & Jastrow 1990). It is worth remarking that if this estimate of the occurrence of grand minima is at all near the mark, then grand minima must be a fundamental property of non-linear stellar dynamos, and must occur over a considerable range of dynamo parameters.

As described in Section 1, several recent dynamo models have produced, for certain ranges of parameters, phenomena that possess characteristics attributed to a Maunder minimum. There have also been attempts to give a dynamical classification of such minima. Knobloch & Landsberg (1996) identified type 1 modulation, characterized by large changes in parity with modest changes in energy, and type 2 modulation with deep energy minima but only small changes in parity. Knobloch & Landsberg's model consisted of a simple system of coupled ordinary differential equations, but both types of modulation were observed in the partial differential equation (PDE) models of T97 and Tobias (1998), who also showed that grand minima could occur in PDE models with imposed dipolar symmetry (Tobias 1996). These models also show that type 1 and type 2 minima can coincide. This produces grand minima with a reduction in the magnetic energy and a change in parity, thus capturing important aspects of the sunspot record at the Maunder minimum.

A different mechanism for producing grand minima was proposed by Brooke et al. (1998), in which the grand minima were intermittent episodes caused by the gradual growth and collapse of a quadrupolar component of a predominantly dipolar solution. During grand minima, the quadrupolar component interacts with the dipolar component, resulting in an overall dip in magnetic energy. Brooke (1997) and Covas et al. (2000) have shown that this behaviour is an instance of 'in–out' intermittency, a generalization of on–off intermittency (Platt, Spiegel & Tresser 1993a,b). The term 'in–out' refers to the two phases described above, the out-phase where parity is moving very slowly away from dipolar parity, and the in-phase where there is a dip in magnetic energy and a rapid return to a nearly pure dipolar state.

The non-linearity in the models showing 'in–out' behaviour was an instantaneous alpha-quenching mechanism, unlike the models of Tobias and collaborators where the non-linearity was due to a dynamical modulation of the differential rotation via the macroscopic Lorentz force (the Malkus–Proctor effect). Intermittent behaviour can also be demonstrated in alpha-quenching models where the alpha-quenching is governed by a dynamical equation analagous to the extra equation governing the Malkus–Proctor effect. However, since the Malkus–Proctor effect involves the solution of an extra equation governing the evolution of the perturbation to the differential rotation, it introduces a time-scale determined essentially by the Prandtl number, which determines the intervals between the grand minima. On the other hand, for in–out intermittency the interval between grand minima is essentially determined by the length of the out-phase, i.e. how quickly the solutions move away from the pure dipolar state.

In this paper we consider a model with a Malkus–Proctor quenching mechanism, and so we might expect results similar to those of the models of Tobias and collaborators. However, the essence of in–out intermittency is that we can identify an out-phase where the quadrupolar and dipolar components are synchronized (like two locked pendula) and the weaker component is slowly growing (from a dynamical point of view the

phenomenon would be the same if the roles of the quadrupolar and dipolar components were reversed). Thus we may find both types of dynamics in our models, and since they can both plausibly describe a Maunder minimum this would be of considerable theoretical interest (note that we do not here consider using both alpha-quenching and Malkus–Proctor non-linearities together, but see KAR for models with two non-linearities acting simultaneously). Careful observation of sunspot records has recently indicated that the relative strengths of the dipolar and quadrupolar field do appear to oscillate together on a time-scale of approximately 90 yr, at least over the period since 1853 when Carrington began systematic observation of sunspot latitudes and longitudes (Pulkkinen et al. 1999 and references therein). In Section we examine the behaviour of our model in the light of the above considerations.

3 THE DYNAMO CODE

We assume conventionally that the gross behaviour of the large-scale magnetic field can be described by the standard mean field equation

$$\frac{\partial \boldsymbol{B}}{\partial t} = \nabla \times (\boldsymbol{u} \times \boldsymbol{B} + \alpha \boldsymbol{B} - \eta \nabla \times \boldsymbol{B}). \tag{1}$$

Here $\boldsymbol{u} = v\hat{\boldsymbol{\phi}} - \frac{1}{2}\nabla\eta$, where $v = \Omega r \sin\theta$, with respect to spherical polar coordinates r,θ,ϕ, and the term proportional to $\nabla\eta$ represents the effects of turbulent diamagnetism. The mean field coefficients α and η are taken to be scalars.

We set $v = v_0 + v'$, where $v_0 = \Omega_0 r \sin\theta$, and Ω_0 is a prescribed underlying rotation law. v' satisfies

$$\frac{\partial v'}{\partial t} = \frac{(\nabla \times \boldsymbol{B}) \times \boldsymbol{B}}{\mu_0 \rho r \sin\theta} \cdot \hat{\boldsymbol{\phi}} + \nu D^2 v', \tag{2}$$

where D^2 is the operator

$$\frac{\partial^2}{\partial r^2} + \frac{2}{r}\frac{\partial}{\partial r} + \frac{1}{r^2 \sin\theta}\left[\frac{\partial}{\partial\theta}\left(\sin\theta \frac{\partial}{\partial\theta}\right) - \frac{1}{\sin\theta}\right].$$

Prescribing $\Omega_0(r,\theta)$ is equivalent, in principle, to postulating a turbulent Reynolds stress field that maintains the angular velocity Ω_0 – cf. KAR.

The assumption of axisymmetry allows the field $\boldsymbol{B}$ to be split into toroidal and poloidal parts, $\boldsymbol{B} = \boldsymbol{B}_\mathrm{T} + \boldsymbol{B}_\mathrm{P} = B\hat{\boldsymbol{\phi}} + \nabla \times A\hat{\boldsymbol{\phi}}$, and equation (1) thus yields two scalar equations, for A and B. We non-dimensionalize in terms of a length R and time R^2/η_0, where R is the solar radius and η_0 the maximum value of η, and put $\Omega = \Omega^*\tilde{\Omega}$, $\alpha = \alpha_0\tilde{\alpha}$, $\eta = \eta_0\tilde{\eta}$, $\boldsymbol{B} = B_0\tilde{\boldsymbol{B}}$ and $v' = \Omega^* R\tilde{v}'$. This gives the following system of equations:

$$\frac{\partial A}{\partial \tau} = w_r B_\theta - w_\theta B_r + R_\alpha \tilde{\alpha} B + \tilde{\eta} D^2 A, \tag{3}$$

$$\begin{aligned}\frac{\partial B}{\partial \tau} = {} & R_\omega r \sin\theta \boldsymbol{B} \cdot \nabla\Omega - \frac{1}{r}\frac{\partial}{\partial r}(r w_r B) - \frac{1}{r}\frac{\partial}{\partial\theta}(w_\theta B) \\ & + R_\alpha\left(-\tilde{\alpha} D^2 a + \frac{\partial\tilde{\alpha}}{\partial r}B_\theta - \frac{1}{r}\frac{\partial\tilde{\alpha}}{\partial\theta}B_r\right) \\ & + \frac{1}{r^2\sin\theta}\frac{\partial\tilde{\eta}}{\partial\theta}(B\sin\theta) + \frac{1}{r}\frac{\partial\tilde{\eta}}{\partial r}\frac{\partial}{\partial r}(rB) + \tilde{\eta} D^2 B,\end{aligned} \tag{4}$$

$$\frac{\partial v'}{\partial \tau} = \Lambda \frac{\nabla \cdot (\boldsymbol{B} B r \sin\theta)}{\tilde{\rho} r \sin\theta} + P_r D^2 v'. \tag{5}$$

Here $\boldsymbol{w} = -\frac{1}{2}\nabla\eta$, the tildes have been dropped on A, B, v' and r, and all quantities are understood to be dimensionless. The dynamo parameters are $R_\alpha = \alpha_0 R/\eta_0$, $R_\omega = \Omega^* R^2/\eta_0$, $P_r = \nu_0/\eta_0$ and $\tilde{\eta} = \eta/\eta_0$. $\Lambda = B_0^2/\mu_0\rho_0\eta_0\Omega^*$; choosing a value for Λ determines B_0, since $\tilde{\boldsymbol{B}}$ scales as B_0^{-1}, and the physical field $\tilde{\boldsymbol{B}}B_0$ is thus independent of the choice of Λ. This freedom of scaling is typical of systems with a single non-linearity. We arbitrarily put $\Lambda = 10^4$. Ω^* is the solar surface equatorial angular velocity. We assume that the density is constant, and so $\tilde{\rho} = \rho/\rho_0 = 1$.

These equations are solved by a second-order Runge–Kutta method on an $NI \times NJ$ grid over the range $r_0 \le r \le 1$, $0 \le \theta \le \pi$ with uniform spacing in both r and θ. Our standard values were $NI = 61$, $NJ = 101$, but test runs were carried out at higher spatial resolution.

This code, although significantly slower than its predecessor, which used a modified Dufort–Frankel integration scheme (e.g. Brandenburg et al. 1989; Moss, Tuominen & Brandenburg 1990b), has the advantage that it can handle much steeper gradients in α and η. Tests showed satisfactory agreement with the earlier code.

Our computational domain includes the convection zone, assumed to extend over $0.7 \le r \le 1$, and an overshoot region/tachocline in $r_0 \le r \le 0.7$. A realistic model would probably have $r_0 \gtrsim 0.67$, but we set $r_0 = 0.64$, for reasons of computational convenience.

At the surface the boundary condition was that $\boldsymbol{B}$ fitted smoothly on to a vacuum exterior field. Thus $B = 0$, and the boundary values of A are determined globally by a matrix multiplication. At $\theta = 0, \pi$, symmetry conditions imply $A = B = 0$. At $r = r_0$, the base of the computational region, the detailed physics is uncertain. We decided to conserve the angular momentum in the computational region. Given that the angular momentum flux owing to the magnetic stresses out of a region with boundary S is $\int_S (\boldsymbol{B}Br\sin\theta)\cdot \mathrm{d}\boldsymbol{S}$, we set $B = 0$ on $r = r_0$, and, correspondingly, stress-free conditions were used for v'. The condition $\partial A/\partial r = A/\delta$ crudely models A falling to zero at distance δ below $r = r_0$ (cf. Moss, Mestel & Tayler 1990a; Tworkowski et al. 1998). We chose $\delta = 0.03$, but the general nature of the results is insensitive to this choice. Taking $\delta > 0$ is computationally helpful as it reduces somewhat the field gradients near $r = r_0$, although it is not essential.

We monitor the time evolution of the total magnetic energy E, a measure of the perturbation kinetic energy $E_\mathrm{K} = \int \frac{1}{2} v'^2 \,\mathrm{d}V$ (rather than the true kinetic energy, so as not to dilute the signal in the large constant background kinetic energy associated with Ω_0), and the global parity of the magnetic field, defined as

$$P = \frac{E^\mathrm{S} - E^\mathrm{A}}{E^\mathrm{S} + E^\mathrm{A}}, \tag{6}$$

where S and A refer respectively to the parts of the magnetic field that have symmetry or antisymmetry with respect to the equatorial plane (see also Brandenburg et al. 1989; Moss 1999). Thus $P = -1$ corresponds to dipole-like symmetry, and $P = +1$ to quadrupole-like.

4 THE ROTATION LAW

For the major part of this investigation, we took Ω_0 to be given in $0.7 \le r \le 1$ by an interpolation to the *SOHO* data of Kosovichev et al. (1997), supplied by M. Korpi and P. Heikkinen (private communication). At $r = r_0$ we assumed that Ω_0 had become constant, and equal to the surface value at $\theta = \theta_0 = 52°$. This is generally consistent with other recent determinations of the solar rotation law (e.g. Christensen-Dalsgaard & Schou 1988; Tomczyk

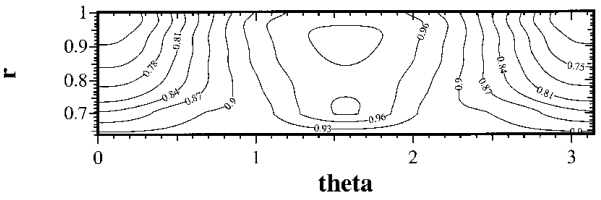

Figure 1. Isorotation contours for the rotation law generated from the *SOHO* data. Contour levels are equally spaced and normalized to a maximum value of unity.

et al. 1995). In $r_0 \leq r \leq 0.7$, we interpolated between the values at $r = r_0$ and $r = 0.7$. Contours of constant Ω_0 are shown in Fig. 1.

We also investigated briefly an alternative, strictly radius-dependent, form of Ω_0, in order to relate our results to those of other authors – see Section 7.

5 THE CHOICE OF α AND η

Basic dynamo theory predicts that when $\alpha\partial\Omega/\partial r > 0$ field migration is poleward, and when $\alpha\partial\Omega/\partial r < 0$ it is equatorward (e.g. Stix 1989). The rotation law of Fig. 1 has $\partial\Omega_0/\partial r > 0$ near the equator, and $\partial\Omega_0/\partial r < 0$ at high latitudes. Thus the correct sense of field migration can only be obtained if $\alpha < 0$ where $|\partial\Omega/\partial r|$ is large, i.e. near the bottom of the convection zone. This decision is made on pragmatic grounds – the main features of the rotation law appear to be reasonably secure, and so if the ideas of mean field dynamo theory have any validity, the sign of alpha is determined in this region.

This is essentially the conclusion of Rüdiger & Brandenburg (1995), who used a tensorial form of alpha, with a negative vertical component. There are certainly both theoretical and numerical grounds for believing that this is not an unreasonable assumption (e.g. Brandenburg et al. 1990; Rüdiger & Kitchatinov 1993; Brandenburg 1994 and references therein).

We write $\tilde{\alpha} = \alpha_r(r)f(\theta)$, where $f(\theta)$ is an odd function with respect to the equator $\theta = \pi/2$. A common choice in the past has been $f(\theta) = \cos\theta$. Experiments showed us that this results in a butterfly diagram that is dominated by a strong polar branch, with a relatively weak equatorial feature. This is explicable, as α has its maximum near the poles. A more satisfactory choice is $f(\theta) = \sin^2\theta\cos\theta$ (cf. Rüdiger & Brandenburg 1995), and we adopt this for all the computations described here.

For $\alpha_r(r)$, the choice

$$\alpha_r = 1; \quad r_{\alpha 1} \leq r \leq r_{\alpha 2}, \tag{7}$$

with cubic interpolation to zero at $r = r_0$ and $r = 1$, satisfies the condition that α be weak in the region of maximum radial rotational shear, where the field is expected to be strong (this is consistent with an implicit acknowledgment that some sort of inhibition of the alpha effect occurs when $|\boldsymbol{B}|$ is large). Moreover, plausible butterfly diagrams are generated, and the numerical behaviour is satisfactory. We have adopted the convention that $\alpha_r > 0$, and so the dynamo number $R_\alpha < 0$.

Experiments with a broadly similar form of $\alpha_r(r)$ in the lower part of the computational region, but that changed sign towards the surface $r = 1$, yielded roughly similar butterfly diagrams, but the general numerical behaviour of these models is less satisfactory. As the aim of this work was to explore the general nature of a superficially plausible dynamo model with dynamical feedback on the differential rotation, we did not pursue the matter further.

Our preliminary computations showed that, for $R_\omega = 6 \times 10^4$, at marginal excitation the cycle period was about 22 yr, whereas for smaller values of R_ω it was shorter. $R_\omega = 6 \times 10^4$ corresponds to $\eta_0 \approx 2.5 \times 10^{11}\ \mathrm{cm^2\ s^{-1}}$, given the known values of Ω^* and R. Then $R_\alpha = \alpha_0 R/\eta \approx 0.3\alpha_0$. The value of α_0 is quite uncertain, but these estimates imply that $|R_\alpha|$ values of 10–100 are readily achievable with only modest values of α_0.

We recognize that the turbulent diffusion coefficient η is likely to be reduced markedly in the overshoot region, and we would have liked to model this. Although the code can formally handle steep η-gradients, in this region they result in steep radial gradients of magnetic field, and this requires higher numerical resolution than we could readily employ. Thus we restricted the variation in η to a rather nominal decrease, to $\tilde{\eta} = 0.5$ in $r < 0.7$, increasing linearly to $\tilde{\eta} = 1$ at $r = 0.8$. With such a modest variation, we did not include the diamagnetic term $-\frac{1}{2}\nabla\tilde{\eta}$ in most of our computations – we did check that its influence was small. Furthermore, experiments with $\tilde{\eta}$ reduced to 0.1 in $r < 0.70$ showed that the cycle period was little affected by the reduction of $\tilde{\eta}$ in a comparatively narrow region. The relation $|\alpha| \propto \mathrm{d}\eta/\mathrm{d}r$ was not modelled (cf. Rüdiger & Brandenburg 1995): we adopted a more pragmatic approach, in common with many previous authors.

Explicit η-quenching was not included. Such an effect arguably requires a tensor representation of the diffusivity (e.g. Kitchatinov, Pipin & Rüdiger 1994), which is beyond the ambitions of this paper.

6 MAIN RESULTS

The most readily excited solutions in linear theory are strictly odd-parity limit cycles, with marginal value $R_{\alpha,c} \approx -3.20$. The even-parity solutions are only slightly harder to excite, with $R_{\alpha,c} \approx -3.25$. We will concentrate on the results with Prandtl number $P_r = 0.01$, as this is plausibly more realistic than larger values, but we also discuss some results for other values of P_r. Our computational procedure was to begin the computations with a field of arbitrarily chosen radial structure and of global parity $P \neq \pm 1$. This field was evolved until transient behaviour appeared to have disappeared. As the dynamical time-scale much exceeds the magnetic diffusion time when $P_r \ll 1$, the transient may be long-lived: see Fig. 2. Indeed, long-lived transients are also found in alpha-quenched dynamos (e.g. Tavakol et al. 1995), although typically for rather more supercritical parameters than found here. We monitored the magnetic energy E, pseudo-kinetic energy E_K and parity P, and examined butterfly diagrams of B_ϕ just below the surface $r = 1$, and in the overshoot region.

6.1 Prandtl number $P_r = 0.01$

For even the slightly supercritical value of $R_\alpha = -3.22$, we found the stable solution to be doubly periodic, with parity $P = -1$. When $R_\alpha = -3.25$, the solution also possesses a long-period modulation: see Fig. 3. For $-3.3 \gtrsim R_\alpha \gtrsim -4$, we found mixed-parity solutions, with intervals in which the field strength had an approximately regular variation, separated by episodes of rapid fluctuations in field strength, and with parity that did not relax to a settled behaviour even after integrating for dimensionless times of order 100. Fig. 4 shows the behaviour with time of such a solution for $R_\alpha = -3.5$. For $-4 \gtrsim R_\alpha \gtrsim -12$, the stable solutions were of

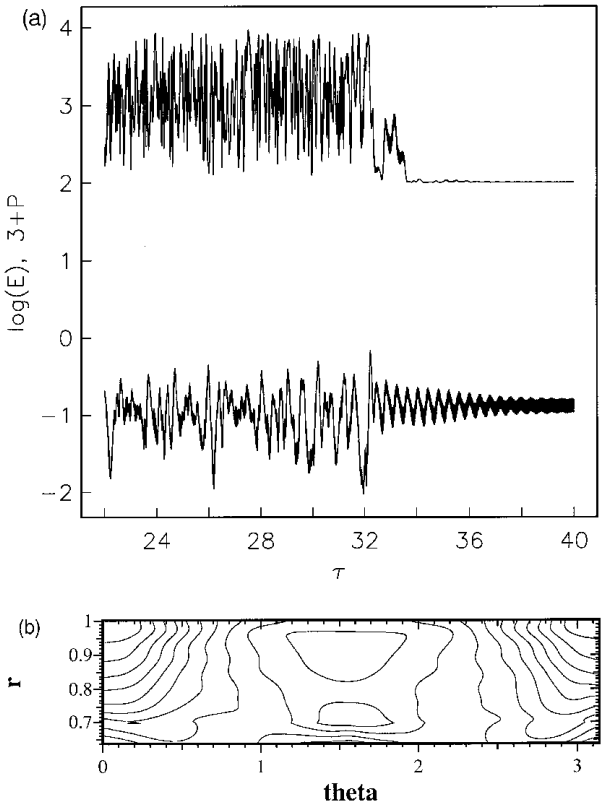

Figure 2. (a) The evolution of magnetic field parity (P) and magnetic energy (E) with time for $P_r = 0.01$, $R_\omega = 6 \times 10^4$, $R_\alpha = -10.0$. Here and in the following figures, the upper curve gives the value of $3 + P$, and the lower that of $\log E$. (b) Typical angular velocity contours.

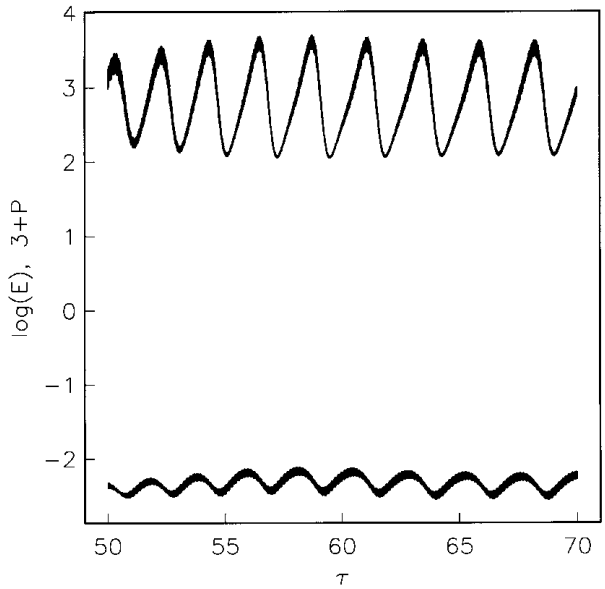

Figure 3. The evolution of magnetic field parity and energy with time for $P_r = 0.01$, $R_\omega = 6 \times 10^4$ and $R_\alpha = -3.25$.

strictly odd parity, and doubly periodic. However, for some parameters (e.g. $R_\alpha = -5$) transient behaviour persisted for approximately 100 time units, with the parity wandering slowly through intermediate values before settling to $P = -1$. For $-12 \gtrsim R_\alpha \gtrsim -40$ (the limit of our investigation), solutions

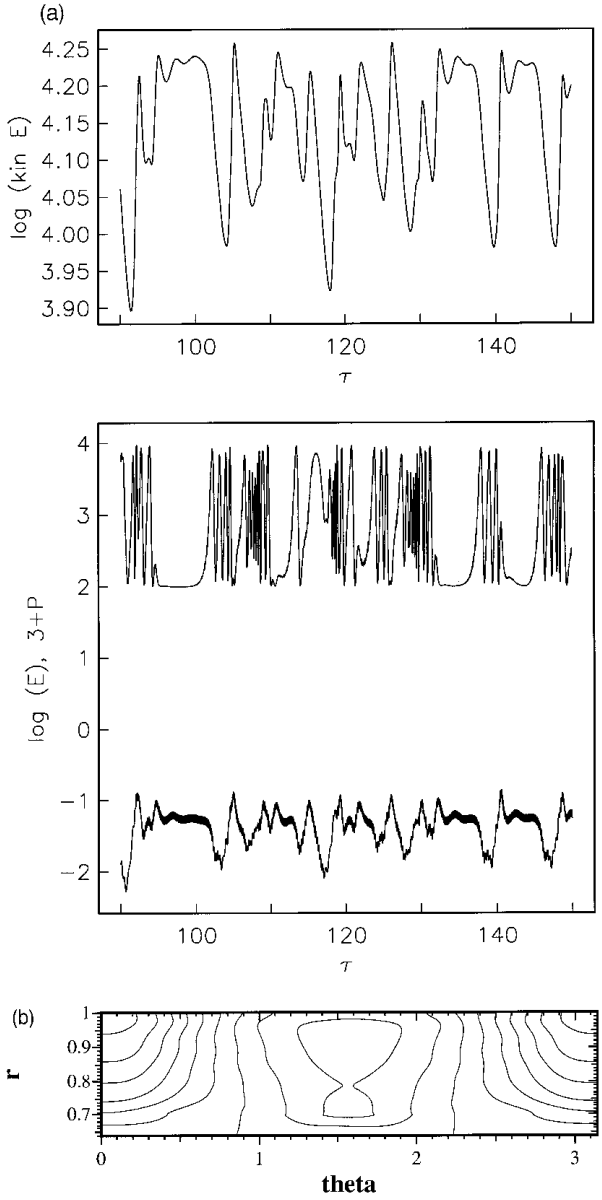

Figure 4. (a) The evolution of pseudo-kinetic energy (E_K) (upper panel) and magnetic field parity and energy (lower panel) with time for $P_r = 0.01$, $R_\omega = 6 \times 10^4$ and $R_\alpha = -3.5$. (b) Typica angular velocity contours.

were irregular in both parity and energy, although for the smaller values of $|R_\alpha|$ in this range there appeared to be an underlying periodicity still present (see Fig. 5).

For values of $|R_\alpha|$ of less than about 20, the magnetic fields are concentrated in the overshoot region (e.g. Fig. 6), and even for larger values the strongest fields are found in the overshoot region and lower parts of the convection zone. Typical maximum and mean strengths (taken over the overshoot region) are about 10^5 and $(2–3) \times 10^4$ G respectively. As the mechanism of formation of sunspots is still uncertain, we show in Fig. 7 butterfly diagrams at the top and bottom of the computational region: they display both polar and equatorial branches.

When $R_\alpha = -40$, the latitudinal migration of field patterns had disappeared. This appears to be a consequence of using an $\alpha^2\omega$ (rather than an $\alpha\omega$) code. With such a large value of $|R_\alpha|$, the α^2 effects have an increased importance. At smaller values of $|R_\alpha|$,

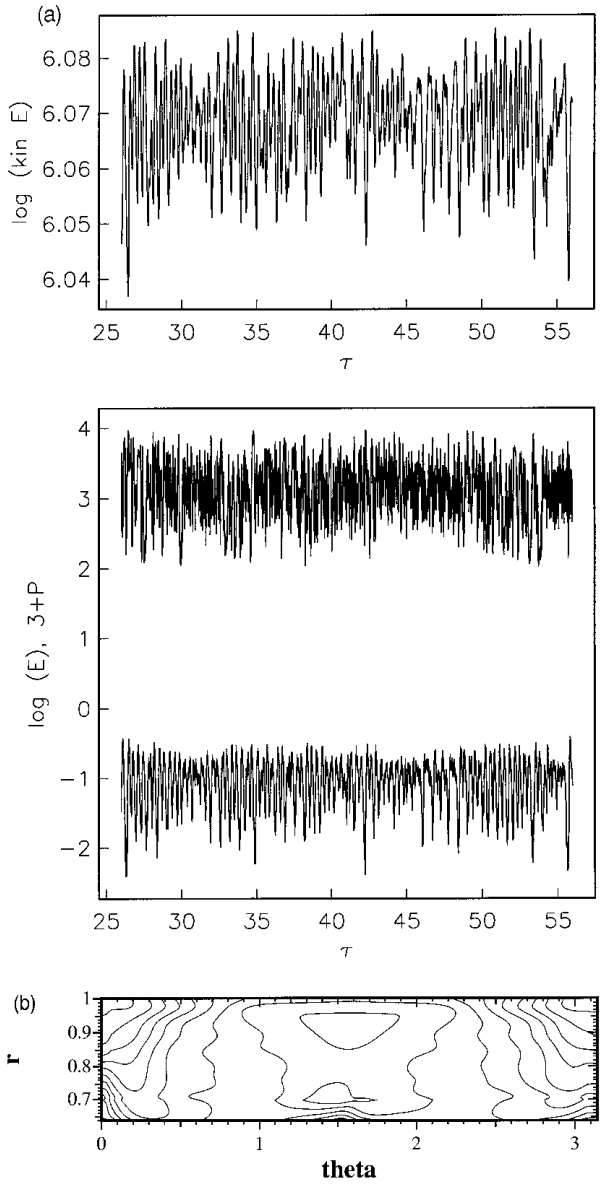

Figure 5. (a) The evolution of pseudo-kinetic energy E_K, magnetic field parity and energy with time for $P_r = 0.01$, $R_\omega = 6 \times 10^4$ and $R_\alpha = -20.0$. (b) Typical angular velocity contours.

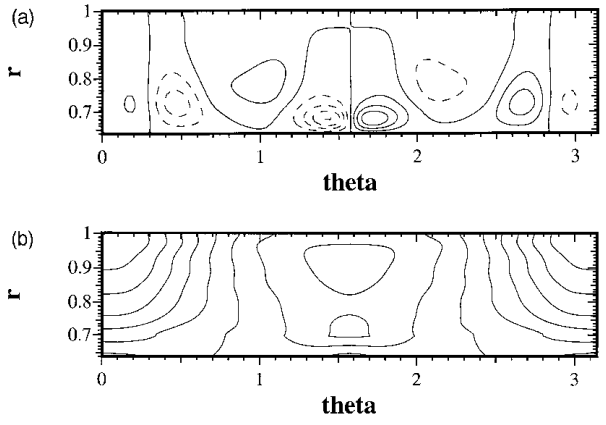

Figure 6. Contours of (a) toroidal field and (b) angular velocity for the model with $P_r = 0.01$, $R_\alpha = -4$ and $R_\omega = 6 \times 10^4$.

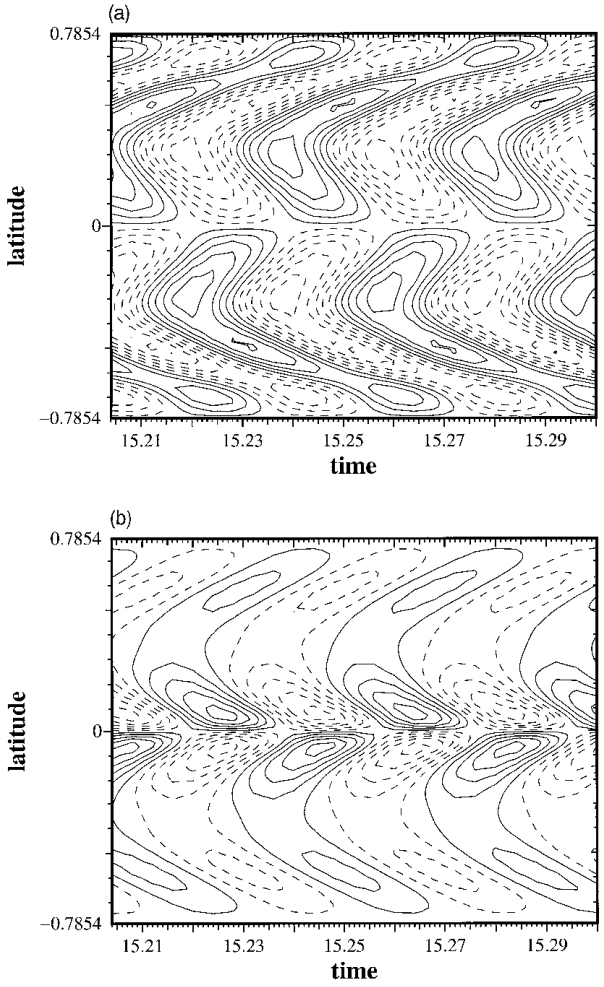

Figure 7. Butterfly diagram of toroidal field for the model with $P_r = 0.01$, $R_\alpha = -4$ and $R_\omega = 6 \times 10^4$: (a) near the top of the convection zone and (b) in the overshoot region. Negative values are indicated by broken contours.

the angular velocity varies only slightly from the underlying Ω_0 field. As $|R_\alpha|$ increases, unsurprisingly these deviations become larger, but the isorotation contours do not differ strongly from those of Ω_0, and probably would be observationally indistinguishable. Certainly for $|R_\alpha| \lesssim 20$, the mean form of Ω over a cycle remains close to Ω_0, and there is no strong variation of Ω with time in any given model. It appears that the time-averaged $\Omega(r,\theta)$ adjusts to the current model parameters, and that, when $|R_\alpha|$ is not too large, subsequent variations about this mean value are small.

We show in Fig. 8 the deviation of the change with time of the angular velocity from the assumed zero-order rotation law of Fig. 1 (normalized to the maximum angular velocity). This is plotted at a point at the top of the 'overshoot region' (fractional radius $r \approx 0.7$), in the middle of the dynamo region, and at the surface of the model, at $\theta \approx 72°$, for intervals from the calculations illustrated in Figs 4, 5 and 10 (later). Only for the calculation with $R_\alpha = -20$ are the variations greater than a few per cent.

6.2 Other values of P_r

We experimented to a limited extent with other values of P_r in the range $1 \geq P_r \geq 0.001$. A general trend was that more 'interesting'

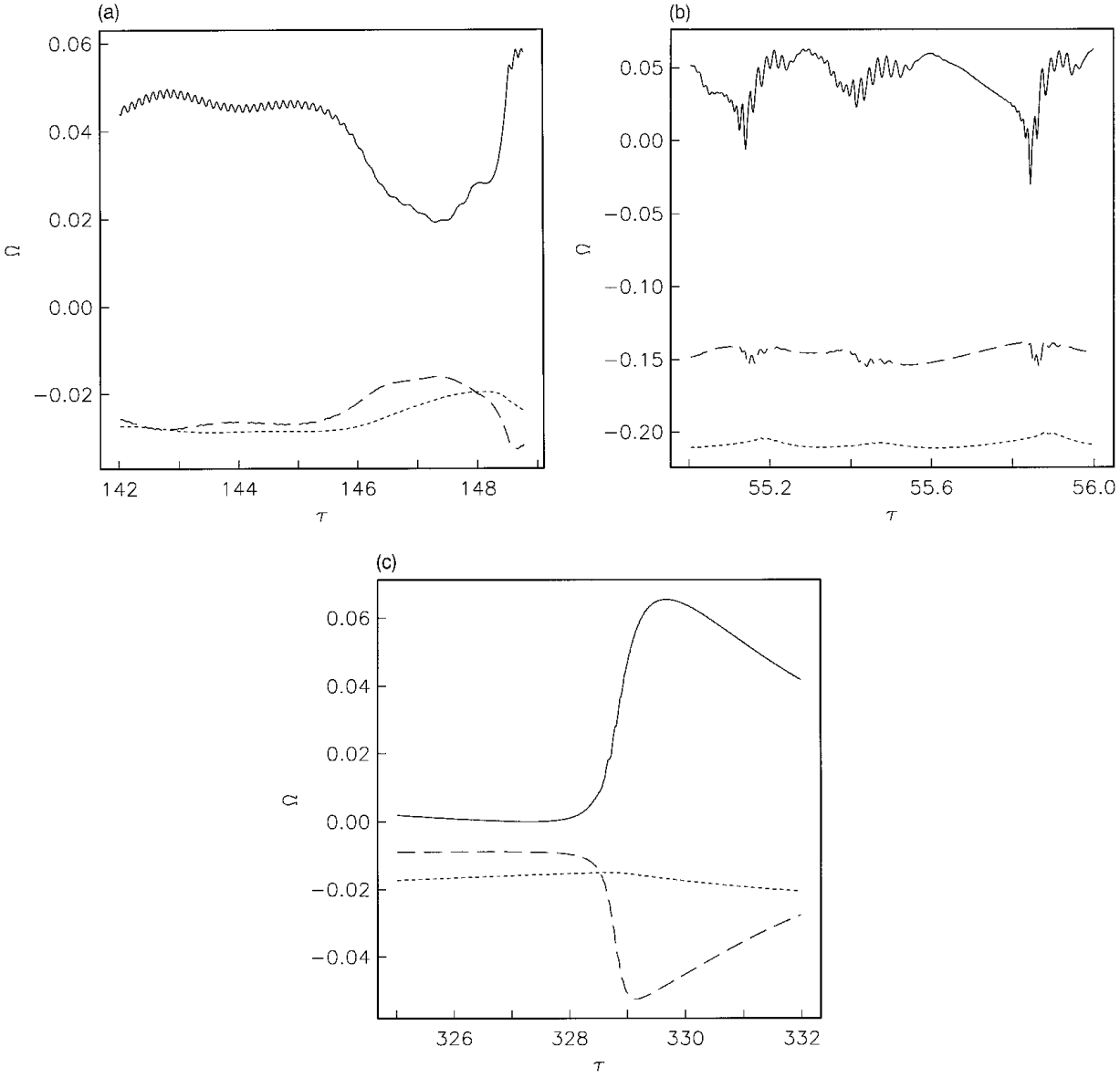

Figure 8. The variation of the normalized perturbations to the angular velocity at the top of the 'overshoot layer' (solid), near the middle of the dynamo region (long-dashed) and at the surface of the model (short-dashed), all at $\theta \approx 72°$. (a) $R_\alpha = -3.5$, $P_r = 0.01$; (b) $R_\alpha = -20$, $P_r = 0.01$; (c) $R_\alpha = -3.5$, $P_r = 0.001$.

dynamical behaviour was found for smaller values of P_r. We show in Figs 9 and 10 the time series for $R_\alpha = -3.5$ when $P_r = 0.1$ and 0.001, to be compared with Fig. 4. Because of the very long dynamical time-scales with $P_r = 0.001$, this was the only case examined with this Prandtl number. When $P_r = 0.1$, we found regular odd-parity solutions in the interval $-4 \lesssim R_\alpha \lesssim -20$: that is, the onset of irregular behaviour occurred at larger values of $|R_\alpha|$ than when $P_r = 0.01$.

7 OTHER CALCULATIONS

We also made a relatively cursory study of a dynamo model in which Ω_0 was a function of r only. We set $\Omega_0(r_0, \theta) = \Omega_S(1, \theta_0)$ (subscript S referring to the *SOHO* data value and $\theta_0 = 52°$), and allowed Ω_0 to increase linearly in $r_0 \leq r \leq 0.71$, and to be constant in $r > 0.71$, thus modelling a tachocline in the overshoot region. Subject to the constraint that the total angular momentum be the same as that as that of the standard zero-order rotation curve described in Section 4, Ω_0 is then determined as a function of r. This procedure is equivalent to the imposition of Reynolds stresses via a Λ-effect (i.e. a mean-field parametrization of the turbulent Reynolds stresses) that depends solely on radius.

Our aim here was twofold. First, we wanted to see if there were generic differences between the main body of our results and those with a radially dependent Ω_0, such as used by a number of other authors. Secondly, we were curious to see whether the Lorentz force would perturb such an $\Omega_0(r)$ to become anything approaching the observed solar rotation law.

We took again $R_\omega = 6 \times 10^4$ (now this gave a cycle period at marginal excitation of approximately 17 yr), and examined only solutions of strictly dipolar parity (i.e. $P = -1$). The marginal value of R_α was now approximately -11. As we increased $|R_\alpha|$ from near the marginal value to about four or five times larger, the non-linear solution was doubly periodic at $R_\alpha = -20$ and -30,

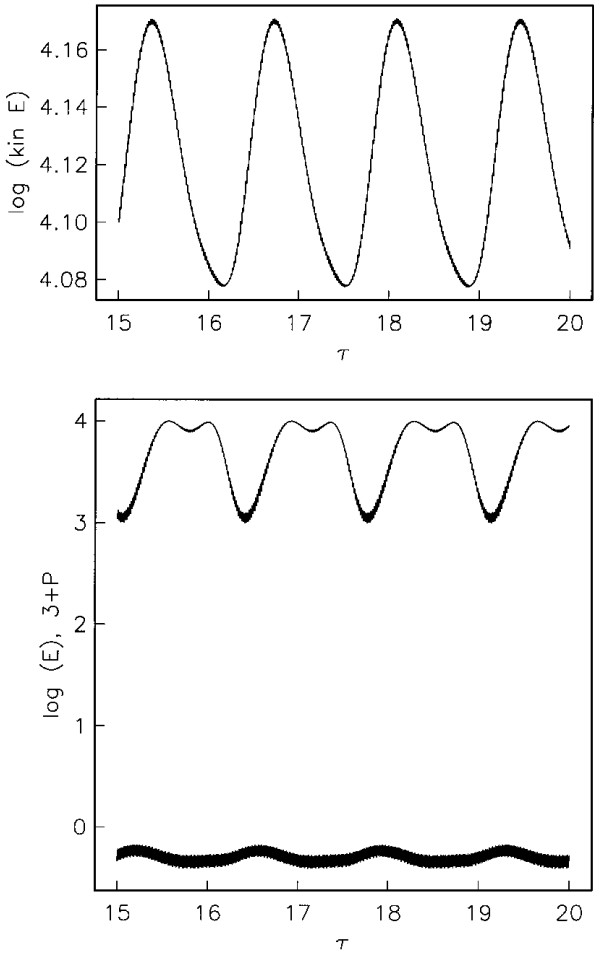

Figure 9. The evolution of pseudo-kinetic energy, magnetic field parity and energy with time for $P_r = 0.1$, $R_\omega = 6 \times 10^4$ and $R_\alpha = -3.5$.

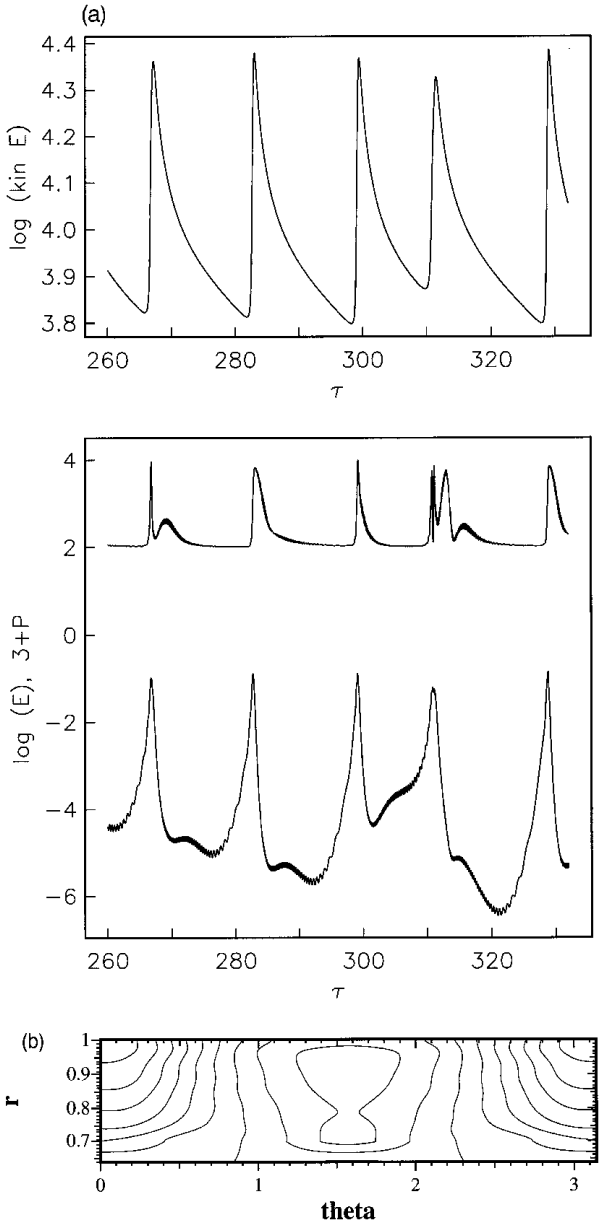

Figure 10. (a) The evolution of E_K, magnetic field parity and energy with time for $P_r = 0.001$, $R_\omega = 6 \times 10^4$ and $R_\alpha = -3.5$. (b) Typical angular velocity contours.

and irregular at $R_\alpha \leq -40$. The most striking feature of the field geometry was that both poloidal and toroidal fields were strongly confined to the region $r_0 \leq r \lesssim 0.7$, and formed four or five belts in each hemisphere: see Fig. 11(a). This was reflected in the butterfly diagrams constructed for the fields both near the top and near the bottom of the computational domain – several activity bands were always present (Fig. 12). Moreover, there was no polar branch. When $R_\alpha = -40$ or -45, the largest values of $|R_\alpha|$ that were used, the latitudinal field migration had ceased near the surface, and had markedly weakened in the overshoot region.

The angular velocity contours are increasingly deformed from the underlying spherical symmetry as $|R_\alpha|$ increases, but even at the largest value considered the variation occurs almost completely in the overshoot region $r_0 \leq r \lesssim 0.70$, and there is only a small surface latitudinal differential rotation: see Fig. 11(b).

The result that a rotation law of the form considered in this section generates a number of latitudinal field belts in each hemisphere is consistent with the work of Moss et al. (1990b), who considered a buoyancy non-linearity in a thin shell model, and of Heikkinen (1997) who used alpha-quenching in a similar model. The model of T97 also implies such a rotation law globally but, as the aspect ratio of the computational region (in Cartesian geometry) corresponds to that of an overshoot region/tachocline of radial extent approximately $0.30R$, i.e. the depth of the convection zone, it is unclear whether or not the global field structures are in agreement with those found here. Similarly, KAR do not display the field geometry of their solutions.

Our conclusion from this brief investigation is that global dynamo models with a radial Ω-gradient confined to a narrow tachocline naturally produce magnetic fields with short latitudinal wavelength, the horizontal length-scale of the field plausibly being determined by that of the angular velocity. Neither the butterfly diagrams nor the rotation laws of such models agree with those observed.

8 ENERGY AND PARITY CHANGES IN THE MODEL

Here we examine the variations in magnetic energy and parity in our results in the light of the discussion of grand minima in

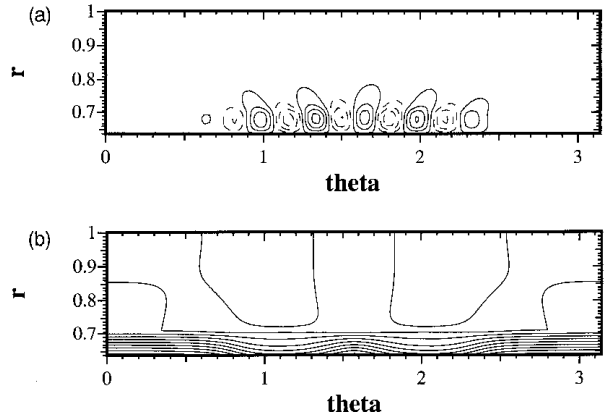

Figure 11. (a) Toroidal field contours (broken contours indicate negative values) and (b) isorotation contours with the radially dependent Ω_0 of Section 7. $R_\alpha = -20$, $R_\omega = 6 \times 10^4$ and $P_r = 0.01$. Contours are uniformly spaced.

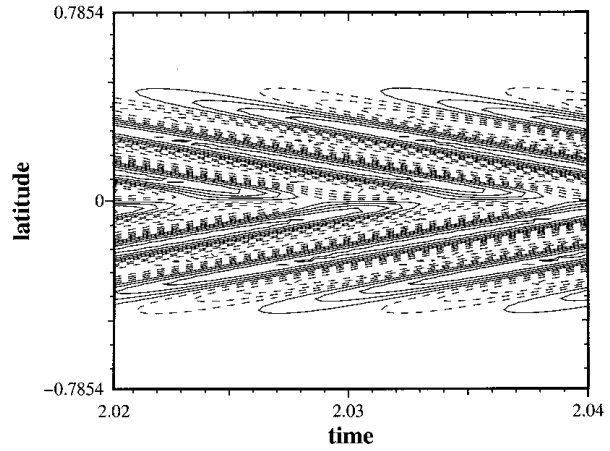

Figure 12. Butterfly diagram of the subsurface toroidal field for the model with $P_r = 0.01$, $R_\alpha = -20$ and $R_\omega = 6 \times 10^4$ with the radially dependent Ω_0 of Section 7.

Section 2. Specifically, we are interested to see if there is any association between spells of reduced magnetic activity and the parity of the solutions. We also consider whether the intervals between grand minima are related to the time-scale changes in the velocity perturbations or to a time-scale related to parity changes. The time-scale of the velocity perturbations can be expected to be related to the Prandtl number (Tobias 1996).

In Fig. 3 we see that the grand minima are correlated with the parity changes, the approach to the minima occurring during the transition from predominantly quadrupolar to predominantly dipolar parity, followed by a rise to 'grand maxima' as the parity change reverses. The actual grand minima and maxima do not coincide with the maxima and minima of parity, thus there is synchronization with a phase-lag. This is clearly the type of behaviour referred to as type 1 modulation by Knobloch & Landsberg 1996. There is no chaos and we have a doubly periodic solution in both parity and energy. There is no intermittency. In Fig. 4 we have exactly the same model parameters except that $|R_\alpha|$ has increased from 3.25 to 3.50. There are three extended episodes where the parity is very close to dipolar, and these coincide with an energy oscillation the amplitude of which remains quite steady. In between these episodes the parity fluctuates between dipolar and quadrupolar, and there are large changes in the amplitude of the energy oscillations. This appears to fit the description of in–out intermittency. To check the predictions of synchronization of quadrupolar and dipolar components in the out-episodes, we decompose the magnetic field into quadrupolar (symmetric) and dipolar (antisymmetric) components as shown in Fig. 13. It can be seen clearly that the changes in both components are synchronized with the magnitude of the quadrupolar field being the mirror image of the dipolar, i.e. as one falls the other rises. This is highly interesting behaviour and fits the predictions of in–out intermittency [see Brooke et al. (1998) for a more extended discussion, where the term 'icicle intermittency' is used for the in–out behaviour]. Furthermore, the interval between grand minima is quite irregular, and there does not appear to be a well-defined time-scale that can be related to the Malkus–Proctor effect.

For the irregular variations in energy and parity present in the time series of Fig. 5, a decomposition of the field into quadrupolar and dipolar components shows that this synchronization has been lost (Fig. 14). Thus such synchronization is not inevitable, and the considerations of the paragraph above show that it appears to have important consequences for the dynamical behaviour of the magnetic energy and parity.

The solutions previously considered had Prandtl number $P_r = 0.01$. If this is reduced to $P_r = 0.001$ we can see clearly that in this case the changes in magnetic energy are now related directly to changes in the velocity field, which occur on a time-scale determined by the azimuthal equation of motion (as in Fig. 10). The parity is now predominantly dipolar except when the velocity pertubations and magnetic energy peak. Decomposing the field as before (Fig. 15), we see clear evidence that changes in the magnitude of the quadrupolar and dipolar components are also synchronized, but are now correlated rather than anticorrelated, although the detailed form of the energy peaks is different for the two components. This behaviour is very suggestive of that of the type 2 modulation described by Knobloch & Landsberg.

Thus we can identify all of the dynamics described in Section 2 as occurring within this one model. If our model is at all representative of solar-type stars, it indicates that they are capable of a rich variety of dynamical behaviour. We also can see that the values of the model parameters, i.e. R_α, R_ω and P_r, can greatly influence the behaviour of the models. (We do not even attempt to study changes with 'hidden' parameters, such as the spatial dependence of α and η.) Since these parameters are not well known, we need to be very careful about over-generalization from a particular model in a particular parameter range. We return to these considerations in Section 9, and intend to address them in more detail in a future publication.

9 DISCUSSION AND CONCLUSIONS

We have attempted to construct a solar dynamo model that incorporates our current knowledge of what is arguably the more important observationally determined information, namely the solar rotation law. In common with several other investigators (e.g. T97; KAR; Pipin 1999), we have used the reaction of the Lorentz force on the rotation as the non-linearity that limits the field at finite amplitude. We differ from many authors in using a realistic, solar-type underlying rotation law, which has a strong latitudinal dependence. In our spherical (rather than Cartesian) geometry, the unperturbed radial shear is largely concentrated in a relatively narrow tachocline. We use stress-free conditions, which conserve angular momentum.

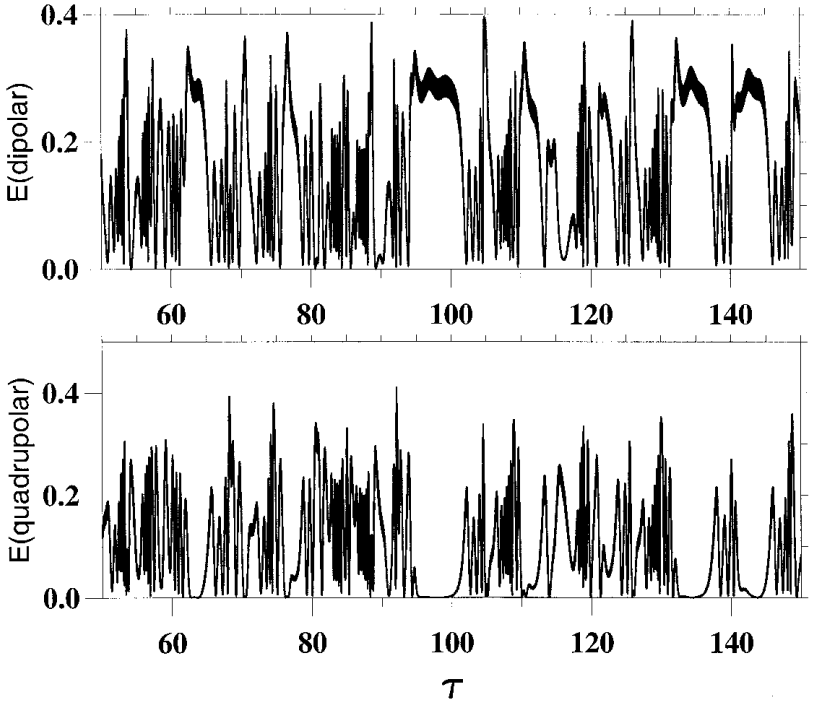

Figure 13. Variations of energy in the antisymmetric (top panel) and symmetric (bottom panel) parts of the magnetic field for $P_r = 0.01$, $R_\alpha = -3.5$ and $R_\omega = 6 \times 10^4$. In this and the two following figures, the curves are thickened by short-period oscillations in energy, which are not resolved on the scale of these figures.

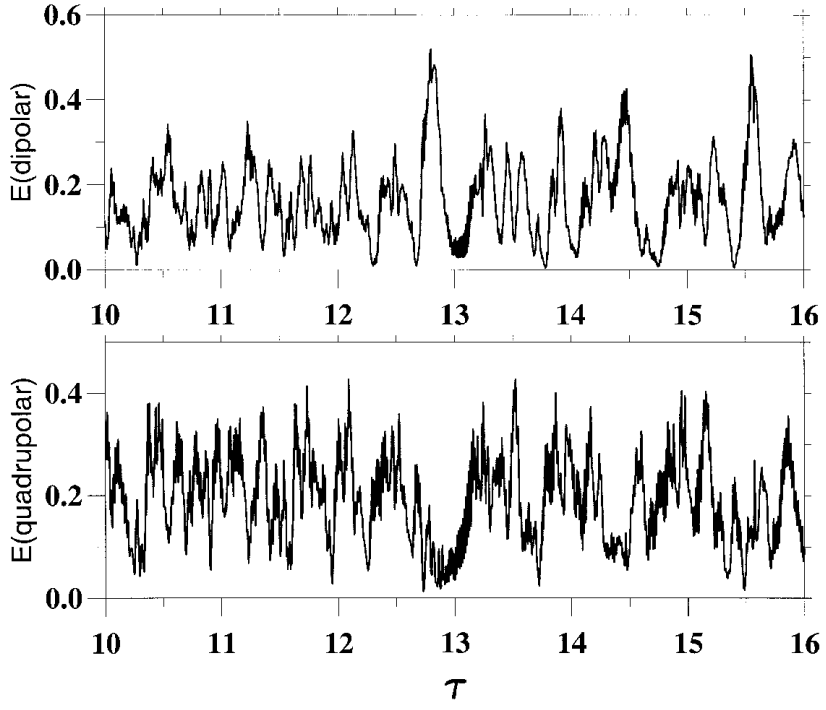

Figure 14. Variations of energy in the antisymmetric (top panel) and symmetric (bottom panel) parts of the magnetic field for $P_r = 0.01$, $R_\alpha = -20$ and $R_\omega = 6 \times 10^4$.

The different assumptions and formulation of the problem by various authors make detailed comparison of results difficult. We mention here just one or two of these factors. T97 does not use stress-free boundary conditions. In the models of both KAR and T97 the unperturbed rotational shear is spread through a comparatively large radial extent. In KAR, the zero-order rotational velocity is independent of latitude, and in T97 the velocity field is quite unsolar in form. The spatial distribution of the alpha coefficient varies between models, and different boundary conditions are applied to the magnetic field. KAR use

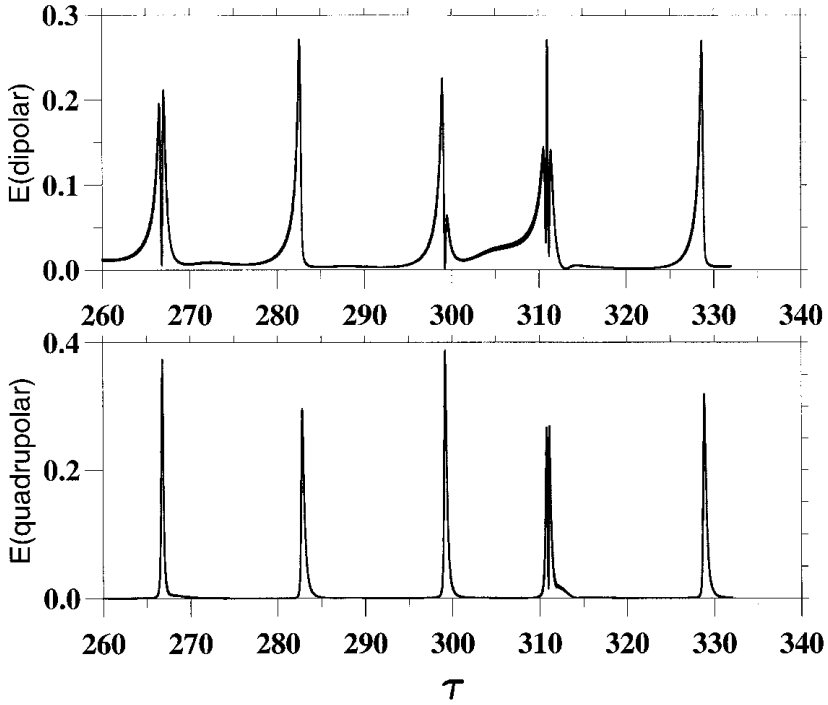

Figure 15. Variations of energy in the antisymmetric (top panel) and symmetric (bottom panel) parts of the magnetic field for $P_r = 0.001$, $R_\alpha = -3.5$ and $R_\omega = 6 \times 10^4$.

a 'Lambda-effect' parametrization of the turbulent Reynolds stresses, and also introduce a second non-linearity, 'Lambda-quenching'.

In common with both T97 and KAR, we do readily find irregular and even intermittent behaviour. Our most convincing examples of intermittent behaviour occur at relatively modest dynamo numbers, with Prandtl numbers $P_r \leq 0.01$. When $P_r = 0.01$ the global magnetic energy falls by 1–2 orders of magnitudes, with associated sudden excursions of the parity from $P \approx -1$ to positive values: e.g. Fig. 4. When $P_r = 0.001$, the intermittency is much more dramatic, with variations of magnetic energy of 3–4 orders of magnitude. Now, however, the dynamo spends most of the time in a low-energy state with $P \approx -1$, with occasional brief excursions to high energy, associated with abrupt increases in parity to near $P = +1$ (Fig. 10). This is explicable by the Lorentz force causing distortions to the angular velocity field, until it reaches a state in which dynamo action is not supported. The magnetic field then decays until the angular velocity diffuses back to near its original state, when approximately exponential growth of the magnetic field occurs, until the Lorentz force is again dynamically significant. As $P_r \ll 1$, this diffusion takes many magnetic diffusion times. It is plausible that the movement of the system into a state where dynamo action cannot occur is more readily accomplished if the dynamo number is not too supercritical. In this case (with $P_r = 0.001$), the behaviour of the energy is almost a mirror image of that of the Sun, in that excursions of parity from $P \approx -1$ are associated with an *enhanced* magnetic energy: see Fig. 10. However, the opposite tendency is visible when $P_r = 0.01$: see Fig. 4.

Thus we differ significantly from T97 and KAR in that we do not believe that we have found long-term behaviour that can convincingly be identified with that of the Sun. However, we reiterate the concerns that we discussed in Sections 1 and 2, that there is considerable uncertainty as to what the essential features of the long-term solar behaviour really are. We recall three crucial questions: does the basic Schwabe cycle continue through a grand minimum, what is the magnitude of the reduction in magnetic activity, and what is the symmetry of the field? There is also the question as to whether there is any linkage between the changes in amplitude, symmetry and cycle length observed on the time-scale of the Gleissberg cycle and the similar but more drastic changes observed in the Maunder minimum. For these reasons, together with questions of the generic nature of the grand minima, we consider that a range of dynamo models with differing rotation laws, boundary conditions and quenching mechanisms need to be investigated thoroughly across a wide range of parameter values. Such investigations can help in the construction of genuinely realistic solar and stellar dynamo models as observations yield more information and computational techniques are able to achieve increasing levels of complexity and resolution. All current models employ drastic approximations in order to be computationally manageable. It is important to compare the effects of these different approximations and to try to understand how they affect the solutions. For instance, our results are substantially different from those of T97, even though we are using the same non-linear quenching mechanism (Malkus–Proctor effect), so questions of curvature, form of rotation law, boundary conditions and aspect ratio of the computational domain are clearly important. KAR find parameter regions and combinations of non-linear effects that produce intermittent behaviour that they associate with grand minima, but it is not clear either how closely these resemble the solar grand minima, or whether these are the only combinations of non-linearities that can achieve such effects.

We find intermittency at low supercriticality (at relatively small Prandtl number), whereas in the T97 model it occurs at 3–4 times supercritical. Some of the results of KAR quite resemble ours, in that the magnetic energy has intermittent peaks, rather than dips. We note that our angular momentum conserving boundary

condition possibly exerts a constraint on energy fluctuations that is absent in the T97 model, and also that, when we set $\Omega_0 = \Omega_0(r)$ (Section 7), the intermittency at low supercriticality was absent.

We note in passing that a double periodicity seems a frequent feature of our models. Close inspection of the figures of KAR suggests that this feature occurs there also, although it is not remarked upon. This could have a connection with long-term periodicities, such as the Gleissberg cycle, reported to be present in the solar record.

Our results do lend support to the conclusion of T97 that, in order to obtain relatively large changes in global field behaviour characteristic of Maunder-type minima, the non-linearity associated with the effect of the azimuthal component of Lorentz force on the rotation law appears to be perhaps the most promising. The introduction of a second time-scale, the comparatively long dynamical scale present when $P_r \ll 1$, seems a natural ingredient of such models. (We note in passing that the assumption $P_r \ll 1$ has yet to be justified by a detailed physical model of turbulent transport processes in solar conditions.) In detail, however, the situation remains unsatisfactory. The simplified model of T97 reproduces some gross features of the dynamical behaviour of the solar dynamo, but with an unrealistic rotation law. It is unclear what would happen to these results if the radial shear were confined to a narrow tachocline. Similar comments can be made about the computations discussed by KAR. Our experiments with a purely radial Ω_0, confined to a relatively narrow layer (Section 7), have unsatisfactory features, and our computations suggest that the detailed form of the rotation law cannot be ignored.

We also note that changes away from $\Omega_0(r)$ in the latter model, caused by the Lorentz force, may be relatively larger than the corresponding changes to $\Omega_S(r, \theta)$ found in the main body of our results. If it is true that equilibration of the model at finite field amplitude can be more readily achieved with the underlying solar-type rotation law, it may be that solutions are more sensitive to changes away from the zero-order rotation law in this case. Arguably, this could be associated with the tendency to obtain intermittent behaviour at low supercriticality. If this conjecture is substantiated, it is a further argument for studying models with rotation laws that accurately represent that of the 'real' Sun.

Whether simplified models can really reproduce the generic dynamical behaviour of the solar field is unclear. We can note here that if it is true that about 30 per cent of solar-type dwarfs exhibit intermittency, then it is not adequate to find a narrow parameter range for which models possess intermittent behaviour. Rather, it must be a quite general property. Of course, for stars other than the Sun we have no information of the behaviour of the parity during a Maunder-type minimum. However, any solar dynamo model that reproduces a plausible long-term behaviour of even the energy alone only within a narrow parameter range is likely to be unsatisfactory from this viewpoint.

We also should recall some of the more obvious deficiencies of our model. In common with all the previous studies cited, we have ignored the controversy about whether the rapid growth of small-scale magnetic fields can limit the growth of the mean field at a magnitude too small to be of astrophysical interest (e.g. Vainshtein & Cattaneo 1992; Cattaneo & Hughes 1996); the matter remains unresolved: see e.g. Brandenburg (1994). However, an alpha effect that is concentrated outside the region of maximum rotational shear and field strength, as used here, does avoid some of any such difficulty (see also Charbonneau & MacGregor 1996). We have ignored the effects of any motions in meridian planes, again in common with almost all previous workers (but see Brandenburg, Moss & Tuominen 1992; Choudhuri, Schüssler & Dikpati 1995). We note that a latitudinal velocity of less than $2\,\mathrm{m\,s^{-1}}$ would advect field at the speed of the equatorward motion of the mean surface activity regions. Thus it is not a priori clear that such effects can be ignored, at least as far as detailed reproduction of the butterfly diagram is concerned. However, their estimation is a delicate matter (e.g. Moss & Vilhu 1983, section 5; Brandenburg et al. 1992), and there is no accepted model. We have not included anisotropies in the coefficients α and η, and have assumed a uniform density when calculating the dynamical feedback on to the rotation field. The latter simplification plausibly may reduce the response of the upper envelope to changes in the magnetic field.

Further uncertainties are associated with the detailed boundary conditions imposed, which are both here and in other models often quite arbitrary, even if physically consistent. We have assumed that the azimuthal Lorentz force provides the sole non-linearity. Although it is plausible that it is important, it cannot be ruled out that other non-linearities (e.g. alpha-quenching, buoyancy, Lambda-quenching) also play a role. For example, it is plausible that alpha-quenching is the effective non-linearity in the upper parts of the convection zone, where the field is relatively weak and the Lorentz force relatively small, whereas lower down the alpha effect is strongly reduced, and modulation of the angular velocity by the Lorentz force dominates. There is also the question of just what properties of the overall solar magnetic field are being monitored by proxies such as sunspot data – it should be remembered that there is as yet no wholly satisfactory model for sunspots. Thus we might consider that the absence of sunspots at the Maunder minimum indicates that the maximum of the field strength never attained a level greater than that associated with the current field at solar minimum. However, the ^{10}Be fluctuations show a vigorous signal with only a modest difference in amplitude from current values (Beer et al. 1998). Thus the absence of sunspots at the Maunder minimum might be more to do with changes in field configuration and radial and latitudinal distribution than with the field amplitude *per se*.

In conclusion, the model discussed in this paper possesses an arguably realistic rotation law and plausible butterfly diagram. For small Prandtl numbers, dynamical behaviour with some of the characteristics of the solar record is produced. Even our idealized model has a relatively complicated behaviour as parameters are varied, and we feel that it is premature for any model to claim to have resolved the problem of the solar intermittency without a reasonably detailed investigation of the relevant parameters. The dynamical behaviour of the system is in general quite rich, and we intend to return to the subject in a later paper. We feel that the claims of other authors to have resolved the problem of explaining the Maunder-type minima in the solar record are somewhat premature. Dynamo models of the sort discussed here and elsewhere do suggest that some basic principles are being addressed, but a number of unsatisfactory features are still present.

ACKNOWLEDGMENTS

We are grateful to P. Heikkinen and M. Korpi for providing a convenient interpolation on the *SOHO* rotation data. We thank an anonymous referee for his/her careful reading of and constructive comments on our paper.

REFERENCES

Ashwin P., Covas E. O., Tavakol R. K., 1999, Non-linearity, 9, 563
Balunias S. L., Jastrow R., 1990, Nat, 348, 520
Beer J., Tobias S. M., Weiss N. O., 1998, Sol. Phys., 181, 237
Brandenburg A., 1994, in Proctor M. R. E., Gilbert A. D., eds, Lectures in Solar and Planetary Dynamos. Cambridge Univ. Press, Cambridge, p. 117
Brandenburg A., Krause F., Meinel R., Moss D., Tuominen I., 1989, A&A, 213, 411
Brandenburg A., Nordlund A., Pulkinnen P., Stein R. F., Tuominen I., 1990, A&A, 232, 277
Brandenburg A., Moss D., Tuominen I., 1992, A&A, 265, 843
Brooke J. M., 1997, Europhys. Lett., 37, 171
Brooke J. M., Pelt J., Tavakol R., Tworkowski A., 1998, A&A, 32, 339
Cattaneo F., Hughes D. W., 1996, Phys. Rev. E, 54, R4532
Charbonneau P., MacGregor K. R., 1996, ApJ, 473, L59
Charbonneau P., MacGregor K. R., 1997, ApJ, 486, 502
Choudhuri A. R., Schüssler M., Dikpati M., 1995, A&A, 303, L29
Christensen-Dalsgaard J., Schou J., 1988, in Domingo V., Rolfe E. J., eds, Seismology of the Sun and Sun-like Stars, ESA SP-286. ESA, Noordwijk, p. 149
Covas E. O., Tavakol R. K., Ashwin P., Tworkowski A. S., Brooke J. M., 2000, Phys. Rev. E, submitted
Heikkinen P., 1997, Pro Grad U thesis, University of Oulu
Kitchatinov L. L., Pipin V. V., Rüdiger R., 1994, Astron. Nachr., 315, 157
Knobloch E., Landsberg A. S., 1996, MNRAS, 278, 294
Knobloch E., Tobias S. M., Weiss N. O., 1998, MNRAS, 297, 1123
Kosovichev A. G. et al., 1997, Sol. Phys., 170, 43
Küker M., Arlt R., Rüdiger G., 1999, A&A, 343, 977 (KAR)
Moss D., 1999, MNRAS, 306, 300
Moss D., Vilhu O., 1983, A&A, 119, 47
Moss D., Mestel L., Tayler R. J., 1990a, MNRAS, 245, 550
Moss D., Tuominen I., Brandenburg I., 1990b, A&A, 240, 142
Parker E. N., 1955, ApJ, 122, 293
Pipin V. V., 1999, A&A, 346, 295
Platt N., Spiegel E. A., Tresser C., 1993a, Phys. Rev. Lett., 70, 279
Platt N., Spiegel E. A., Tresser C., 1993b, Geophys. Astrophys. Fluid Dyn., 73, 147
Pulkkinen P., Brooke J., Pelt J., Tuominen I., 1999, A&A, 341, L43
Ribes J. C., Nesme-Ribes E., 1993, A&A, 276, 549
Roald C. B., Thomas J. H., 1997, MNRAS, 288, 551
Rüdiger G., Brandenburg A., 1995, A&A, 296, 557
Rüdiger R., Kitchatinov L. L., 1993, A&A, 269, 581
Schmitt D., Schüssler M., Ferris-Mas A. A., 1996, A&A, 311, L1
Sokoloff D. D., Nesme-Ribes E., 1994, A&A, 288, 293
Steenbeck M., Krause F., Rädler K.-H., 1966, Z. Naturforsch., 21a, 369
Stix M., 1989, The Sun. Springer-Verlag, Berlin
Struiver M., Braziunas T. F., 1989, Nat, 338, 405
Tavakol R., Tworkowski A., Moss D., Tuominen I., 1995, A&A, 296, 269
Tobias S. M., 1996, ApJ, 467, 870
Tobias S. M., 1997, A&A, 322, 1007 (T97)
Tobias S. M., 1998, MNRAS, 296, 653
Tomczyk S., Schou T., Thompson M. J., 1995, ApJ, 448, L57
Tworkowski A., Tavakol R., Brooke J. M., Moss D., Tuominen I., 1998, MNRAS, 296, 287
Vainshtein S. I., Cattaneo F., 1992, ApJ, 393, 165
Verma V. K., 1993, ApJ, 403, 797

This paper has been typeset from a TEX/LATEX file prepared by the author.